Sliding Input Output Control of Squirrel Cage Motor Based NPC Five Level Inverter

Kheira Mendaz[1*], Houcine Miloudi[2], Khadidja Younes[3]

[1] IRECOM Laboratory, Department of Electrical Engineering, Faculty of Science and Technology, University of Belhadj Bouchaib Ain Temouchent, N101 Route de Sidi Bel Abbes, 46000 Ain Temouchent, Algeria
[2] APELEC Laboratory, Electrical Engineering Department, School of Engineering Science, Djillali Liabes University, 22000 Sidi Bel Abbes, P.O.B. 89, Algeria
[3] Department of Electrical Engineering, Faculty of Science and technology, University of Belhadj Bouchaib Ain Temouchent, N101 Route de Sidi Bel Abbes, 46000 Ain Temouchent, Algeria
* Corresponding author, e-mail: kheira.mendaz@univ-temouchent.edu.dz

Abstract

Speed squirrel cage motor control is an area of research that has been in evidence for some time now. In this paper, a nonlinear controller is presented for the squirrel cage motor drives, based on a combination between input-output feedback linearization control (IOLC) technique and sliding mode control (SMC) to create a new control which is sliding input-output linearization (SIOLC) control of squirrel cage motors which associates by an NPC five levels inverter PWM technical used for the variation of its speed, where the sliding mode control it used for controlling the speed of squirrel cage motor and the input-output linearization control applied for two input witch are flux and current. To test robustness and performance of sliding input-output linearization control (SIOLC) we created a variation of internal parameters of the motor. The simulation results show robustness the sliding input-output linearization control of squirrel cage motor responses.

Keywords

squirrel cage motor, NPC five levels inverter, sliding mode control, input-output linearization control, robustness

1 Introduction

Squirrel cage motor is one of most machines used in most variable speed applications, because it has certain advantages, such as ease of manufacture and maintenance. It is also appreciated for its reliability and robustness. However, the simplicity of its mechanical structure is accompanied by a high complexity in the mathematical model (multi-variable and non-linear) [1, 2].

Due to the significant influence of nonlinearities on squirrel cage motor system dynamics, linear control techniques are quite good, and they may not meet the system specifications, mainly in the case of variable speed applications. Among these nonlinear techniques that ensure high performance and global decoupling between the outputs to control whatever the path profile imposed for the machine, one can mention the input-output linearization technique and the other is sliding mode technique [3–8].

The input-output linearization control is an analytical design approach which aims to reduce the original nonlinear problem to a simpler linear control problem. The nonlinear control system is designed using a two-step procedure [3, 4].

Firstly, a nonlinear process model is used to synthesize a nonlinear state feedback controller that linearized the map between a new manipulated input and the controlled output. In the second step, a linear pole placement controller is designed for the feedback linearized system.

The basic principle of sliding mode control consists in moving the state trajectory of the system toward a predetermined surface called sliding or switching surface and in maintaining it around this latter with an appropriate switching logic. The design of a sliding mode controller has two steps, namely, the definition of the adequate switching surface and the development of the control law (equivalent command and discontinuous command). The sliding mode control can offer good properties, such as insensitivity to parameter variations [9–17].

Multilevel inverter offers interesting advantages such as possibility of operation in medium, high voltage and high-power applications, providing a better voltage waveform with low total harmonic distortion for electric machines applications [18, 19].

This article discus about combination between two nonlinear controls which are input-output linearization control and sliding mode control of squirrel cage motors which associates by an NPC five levels inverter PWM technical used for the variation of its speed.

2 Modeling of squirrel cage motor in dq rotating

The mathematical model of the squirrel cage motor is used for analyzing the dynamic behavior of the motor. The change in the dynamic behavior of the motor affects the motor parameters such as speed, torque, resistance, flux analyzing the change in performance of squirrel cage motor (see in the Appendix). Dynamic model of squirrel cage motor is derived by transforming the three-phase quantities into two phase's axes quantities (Park transforms). Mathematical equation of squirrel cage motor is given below (dq rotating) wish rewritten in rotation reference frame [8, 9]:

$$\frac{d\Omega}{dt} = \frac{T_e}{J} - \frac{1}{J}T_l - \frac{1}{J}f\Omega, \tag{1}$$

$$\frac{dI_{sd}}{dt} = -\lambda I_{sd} + w_s I_{sq} + \frac{K}{\tau_r}\varphi_{rq} + w_r K\varphi_{rd} + \frac{1}{\sigma L_s}V_{sd}, \tag{2}$$

$$\frac{dI_{sq}}{dt} = -w_s I_{sd} - \lambda I_{sq} - w_r K\varphi_{rd} - \frac{K}{\tau_r}\varphi_{rq} + \frac{1}{\sigma L_s}V_{sq}, \tag{3}$$

$$\frac{d\varphi_{rd}}{dt} = \frac{L_m}{\tau_r}I_{sd} - \frac{1}{\tau_r}\varphi_{rd} + (w_s - w_r)\varphi_{rq}, \tag{4}$$

$$\frac{d\varphi_{rq}}{dt} = \frac{L_m}{\tau_r}I_{sq} - (w_s - w_r)\varphi_{rd} - \frac{1}{\tau_r}\varphi_{rq}, \tag{5}$$

where T_e is the electromagnetic torque (N m), T_l is load torque (N m), f is viscous friction coefficient (N m (rd/s)$^{-1}$), w_s is stator pulsation (rd/s); w_r rotor pulsation (rd/s); with:

$$\tau_r = \frac{L_r}{R_r}, \;\; \sigma = 1 - \frac{L_m^2}{L_s L_r}, \;\; T_e = \frac{pL_m}{JL_r}(\varphi_{rd}I_{sq} - \varphi_{rq}I_{sd}),$$

where σ is the scattering coefficient Blondel.

3 Input-output linearization control of squirrel cage motor

The choice of outputs is according to the objectives of control. The current is chosen as the first output while the second output selected is the square of the rotor flux, so as for tracking the purposed control trajectory [10, 11].

$$y(x) = \begin{bmatrix} h_1(x) \\ h_2(x) \end{bmatrix} = \begin{bmatrix} I_{sq} \\ \varphi_{dr}^2 + \varphi_{qr}^2 \end{bmatrix} \tag{6}$$

The time derivative of the system output $h_1(x)$ can be expressed as:

$$y_1 = h_1(x) = I_{sq}, \tag{7}$$

$$\frac{dy_1}{dt} = \frac{dh_1(x)}{dt} = \frac{dI_{sq}}{dt}, \tag{8}$$

$$\frac{dy_1}{dt} = L_f h_1(x) + L_{g1} h_1(x) V_{sd} + L_{g2} h_1(x) V_{sq}, \tag{9}$$

$$\frac{dy_1}{dt} = -w_s I_{sd} - \lambda I_{sq} - w_r K\varphi_{rd} - \frac{K}{\tau_r}\varphi_{rq} + \frac{1}{\sigma L_s}V_{sq}. \tag{10}$$

The degree of $h_1(x)$ is $r_1 = 1$.

The time derivative of the system output $h_2(x)$ can be expressed as:

$$y_2 = h_2(x) = \varphi_r^2, \tag{11}$$

$$\frac{dy_2}{dt} = \frac{dh_2(x)}{dt} = \frac{d\varphi_r^2}{dt}, \tag{12}$$

$$\frac{dy_2}{dt} = L_f h_2(x) + L_{g1} h_2(x) U_{sd} + L_{g2} h_2(x) U_{sq}, \tag{13}$$

$$\varphi_r^2 = \varphi_{rd}^2 + \varphi_{rq}^2, \tag{14}$$

$$\varphi_r^2 = \frac{2}{\tau_r}\left(L_m\left(\varphi_{dr}I_{sq} + \varphi_{qr}I_{sd}\right) - \left(\varphi_{rd}^2 + \varphi_{rq}^2\right)\right). \tag{15}$$

Note that for a controllable system, the total relative degree is defined as the sum of all the relative degrees, it must be less than or equal to the system order, $r \leq n$; with « n » as the system order, and r is total relative degree [6, 7].

In the case of the squirrel cage motor system, it is easy to verify that the control can't appear for the first time

in the first derivative of the outputs y_2 so we derivative the outputs dy_2/dt for the second time that presented in Eqs. (16)–(18) [10]:

$$\frac{d^2 y_2}{dt^2} = \frac{d^2 h_2(x)}{dt^2} = \frac{d^2 \varphi_r^2}{dt^2}, \tag{16}$$

$$\frac{d^2 y_2}{dt^2} = L_f^2 h_2(x) + L_{g1} L_f h_2(x) V_{sd} + L_{g2} L_f h_2(x) V_{sq}, \tag{17}$$

$$\frac{d^2 y_2}{dt^2} = \left(2 \left(\frac{1}{\tau_r} \right)^2 (2 + k L_m) \right)(\varphi_{rd}^2 + \varphi_{rq}^2)$$
$$+ \left(\frac{2 n_p L_m}{\tau_r} \right)(\Omega(\varphi_{rd} I_{sq} + \varphi_{dr} I_{sq}))$$
$$- \left(\left(6 \left(\frac{1}{\tau_r} \right)^2 L_m \right) + \left(\frac{2 \lambda L_m}{\tau_r} \right) \right)(\varphi_{rd} I_{sq} + \varphi_{dr} I_{sd}) \tag{18}$$
$$+ \left(2 \left(\frac{L_m}{\tau_r} \right)^2 \right)(I_{sd}^2 + I_{sq}^2) + \frac{2 p L_m^2}{J L_r \sigma L_s} \varphi_{dr} V_{sd}$$
$$+ \frac{2 p L_m^2}{J L_r \sigma L_s} \varphi_{rq} V_{sq}.$$

The degree of $h_2(x)$ is $r_2 = 2$.

The global relative degree is lower than the order n of the system $r = r_1 + r_2 = 3 < n < 5$.

The relation between the input (V_{sd}, V_{sq}) and the output (y_1, y_2) is given by Eq. (19):

$$\begin{bmatrix} \dfrac{d^2 y_1}{dt^2} \\ \dfrac{d^2 y_2}{dt^2} \end{bmatrix} = A(x) + D(x) \begin{bmatrix} V_{ds} \\ V_{qs} \end{bmatrix}, \tag{19}$$

$$A(x) = \begin{bmatrix} L_f h_1(x) \\ L_f^2 h_2(x) \end{bmatrix}, \tag{20}$$

$$L_f h_1(x) = -w_s I_{sd} - \lambda I_{sq} - w_r K \varphi_{rd} - \frac{K}{\tau_r} \varphi_{rq}, \tag{21}$$

$$L_f^2 h_2(x) = \left(2 \left(\frac{1}{\tau_r} \right)^2 (2 + k L_m) \right)(\varphi_{rd}^2 + \varphi_{rq}^2)$$
$$+ \left(\frac{2 p L_m}{\tau_r} \right)(\Omega(\varphi_{rd} I_{sq} + \varphi_{dr} I_{sq}))$$
$$- \left(\left(6 \left(\frac{1}{\tau_r} \right)^2 L_m \right) + \left(\frac{2 \lambda L_m}{\tau_r} \right) \right)(\varphi_{rq} I_{sq} + \varphi_{dr} I_{sd}) \tag{22}$$
$$+ \left(2 \left(\frac{L_m}{\tau_r} \right)^2 \right)(I_{sd}^2 + I_{sq}^2),$$

$$D(x) = \begin{bmatrix} L_{g1} L_f h_1 & L_{g2} L_f h_1 \\ L_{g1} L_f h_2 & L_{g2} L_f h_2 \end{bmatrix}, \tag{23}$$

$$D(x) = \begin{bmatrix} 0 & \dfrac{1}{\sigma L_s} \\ \dfrac{2 p L_m^2}{J L_r \sigma L_s} \varphi dr & \dfrac{2 p L_m^2}{J L_r \sigma L_s} \varphi_{rq} \end{bmatrix}. \tag{24}$$

The nonlinear feedback provides to the system a linear comportment input/output:

$$\begin{bmatrix} \dfrac{dy_1}{dt} \\ \dfrac{d^2 y_2}{dt^2} \end{bmatrix} = \begin{bmatrix} v_1 \\ v_2 \end{bmatrix}, \tag{25}$$

$$\begin{bmatrix} V_{ds} \\ V_{qs} \end{bmatrix} = D^{-1}(x) \begin{bmatrix} v_1 - L_f h_1(x) \\ v_2 - L_f^2 h_2(x) \end{bmatrix}. \tag{26}$$

4 Current and flux linear control
The internal inputs (V_1, V_2) are definite [9, 10]:

$$V_1 = \frac{dh_1(x)}{dt} = \frac{dI_{sq}}{dt}, \tag{27}$$

$$V_2 = \frac{d^2 y_2}{dt^2} = \frac{d^2 \varphi_r^2}{dt^2}, \tag{28}$$

$$V_1 = \frac{de_1}{dt} + K_{11} e_1, \tag{29}$$

$$V_2 = \frac{d^2 e_2}{dt^2} + K_{21} \frac{de_2}{dt} + K_{22} e_2, \tag{30}$$

$$V_1 = \left(\frac{dI_{sqref}}{dt} - \frac{dI_{sq}}{dt} \right) + K_{11} \left(I_{sqref} - I_{sq} \right), \tag{31}$$

$$V_2 = \left(\frac{d^2 \varphi_{rref}^2}{dt^2} - \frac{d\varphi_r^2}{dt} \right)$$
$$+ K_{21} \left(\frac{d\varphi_{rref}^2}{dt} - \frac{d\varphi_r^2}{dt} \right) + K_{22} \left(\varphi_{rref}^2 - \varphi_r^2 \right). \tag{32}$$

The error of the track is given by flowing equation:

$$\frac{de_1}{dt} + K_{11} e_1 = 0, \tag{33}$$

$$\frac{d^2 e_2}{dt^2} + K_{21} \frac{de_2}{dt} + K_{22} e_2 = 0, \tag{34}$$

$$e_1 = I_{sqref} - I_{sq}, \tag{35}$$

$$\frac{de_1}{dt} = \frac{dI_{sqref}}{dt} - \frac{dI_{sq}}{dt}, \tag{36}$$

$$e_2 = \varphi_{rref}^2 - \varphi_r^2, \tag{37}$$

$$\frac{de_2}{dt} = \frac{d\varphi_{rref}^2}{dt} - \frac{d\varphi_r^2}{dt}, \tag{38}$$

$$\begin{bmatrix} V_{ds} \\ V_{qs} \end{bmatrix} = D^{-1}(x) \begin{bmatrix} v_1 - L_f h_1(x) \\ v_2 - L_f^2 h_2(x) \end{bmatrix}$$
$$= \begin{bmatrix} \left(\dfrac{dI_{sqref}}{dt} - \dfrac{dI_{sq}}{dt} \right) + K_{11} \left(I_{sqref} - I_{sq} \right) \\ -L_f h_1(x) \dfrac{d^2 \varphi_{rref}^2}{dt^2} + K_{21} \left(\dfrac{d\varphi_{rref}^2}{dt} - \dfrac{d\varphi_r^2}{dt} \right) \\ + K_{22} \left(\varphi_{rref}^2 - \varphi_r^2 \right) - L_f^2 h_2(x) \end{bmatrix}, \tag{39}$$

where the coefficients K_{11}, K_{21} and K_{22} are choosing to satisfy asymptotic stability and excellent tracking [1]:

$$\left(\frac{dI_{sqref}}{dt} - \frac{dI_{sq}}{dt} \right) + K_{11} \left(I_{sqref} - I_{sq} \right) = 0, \tag{40}$$

$$\left(\frac{d^2 \varphi_{rref}^2}{dt^2} - \frac{d\varphi_r^2}{dt} \right) + K_{21} \left(\frac{d\varphi_{rref}^2}{dt} + \frac{d\varphi_r^2}{dt} \right)$$
$$+ K_{22} \left(\varphi_{rref}^2 - \varphi_r^2 \right) = 0, \tag{41}$$

where:

$$\frac{dI_{sqref}}{dt} = 0, \quad \frac{d^2 \varphi_{rref}^2}{dt^2} = 0, \quad \frac{d\varphi_{rref}^2}{dt} = 0.$$

From this we can see that:

$$\frac{dI_{sq}}{dt} + K_{11} I_{sq} = K_{11} I_{sqref}, \tag{42}$$

$$\frac{d_2 \varphi_r^2}{dt_2} + K_{21} \frac{d\varphi_r^2}{dt} + K_{22} \varphi_r^2 = K_{22} \varphi_{rref}^2. \tag{43}$$

From Eq. (42) and Eq. (43) the current and flux transfer function given by Eqs. (44) and (45):

$$\frac{I_{sq}}{I_{sqref}} = \frac{1}{1 + \dfrac{1}{K_{11}} p}, \tag{44}$$

$$\frac{\varphi_r^2}{\varphi_{rref}^2} = \frac{K_{22}}{K_{22} + K_{21} p + p_2}. \tag{45}$$

In closed loops, the current transfer functions have first-order dynamics:

$$FT_1 = \frac{K}{1 + Tp}. \tag{46}$$

In closed loops, flux transfer functions have second-order dynamics:

$$FT_2 = \frac{\omega_n}{\omega_{n2}^2 + 2\varepsilon \omega_{n2} p + p_2}. \tag{47}$$

From Eq. (44) and Eq. (46) and with identification:

$$T = \frac{1}{K_{11}} \Rightarrow K_{11} = \frac{1}{T} = \frac{3}{T_r}, \tag{48}$$

with $T_r = 3\,T(\pm 5\%)$, where T_r is the response time, and T is the time constant.

From this we can see that:

$$T_r = \frac{1}{\varepsilon \omega_{n1}}, \tag{49}$$

$$T = \frac{T_r}{3} = \frac{1}{3\varepsilon \omega_{n1}}, \tag{50}$$

$$K_{11} = 3\varepsilon \omega_{n1}, \tag{51}$$

with $\omega_{n1} = 30$ rd/s, $\varepsilon = 1$, the value of K_{11} will be: $K_{11} = 60$.

From Eq. (45) and Eq. (47) and with identification:

$$\begin{cases} K_{21} = 2\varepsilon \omega_n \\ K_{22} = \omega n^2 \end{cases}, \tag{52}$$

with $\omega_{n2} = 60$ rd/s, the values of K_{21} and K_{22} will be:

$$\begin{cases} K_{21} = 120 \\ K_{22} = 3600 \end{cases}.$$

5 NPC five level inverter

In conventional multilevel inverters, the power semiconductor switches are combined to produce a high-frequency waveform in positive and negative polarities.

The general structure of the multilevel inverter is to synthesize a sinusoidal voltage from several levels of voltages, typically obtained from capacitor voltage sources. The multilevel NPC inverter starts from three levels [13–20].

The most commonly used topologies are neutral-point-clamped (NPC). In neutral-point clamped inverter the DC-link is split into many numbers of smaller voltage levels using a series bank connected bulk capacitors. The inverter structure does allow the connections of the

inverter poles to any of these voltage levels, thus creating a multi-level voltage waveform at the output [20].

An NPC three-phase five-level converter have a common DC bus, it consists of eight switches connected in series, six median diodes, each switch consists of an IGBT and an antiparallel diode, four capacitors and one DC voltage source (Fig. 1).

These switches must not be opened or closed simultaneously, in order to avoid a short circuit of the DC source of the input of the inverter, or the opening of the inductive circuit of its load. The floating diodes (six per arm) ensure the application of the different voltage levels at the output of each arm.

The continuous input bus is composed of four capacitors (C_1, C_2, C_3 and C_4), making it possible to create a set of three capacitive middle points. The total voltage of the DC bus is V_{DC}; under normal operating conditions, it is uniformly distributed over the four capacitors, which then have a voltage $V_{DC}/4$ at their terminals [17].

The levels of output voltage are $V_{DC}/2$, $V_{DC}/4$, 0, $-V_{DC}/4$, $-V_{DC}/2$. Although this topology uses only one DC voltage source [14, 15]. A five-level NPC converter is able to produce five levels of line to line voltage and three levels of phase voltage. This NPC converter reduces harmonics in both voltage and current output [12–16].

To obtain the five voltage levels, switches are following switching states as shown in Table 1 [16, 17].

6 NPC pulse width modulation strategy

Among all the available switching strategies, pulse width modulation (PWM) technique is the most desirable choice

Table 1 switch states for NPC five level inverter

K_1	K_2	K_3	K_4	K_1'	K_2'	K_3'	K_4'	Voltage levels
1	1	1	1	0	0	0	0	V_{DC}
0	1	1	1	1	0	0	0	$\dfrac{3V_{DC}}{4}$
0	0	1	1	1	1	0	0	$\dfrac{V_{DC}}{2}$
0	0	0	1	1	1	1	0	0
0	0	0	0	1	1	1	1	$\dfrac{V_{DC}}{4}$

States of switches — header spans K_1 through K_4'

due to its flexibility in switching sequence design to suit various types of inverter topologies. For a multilevel inverter, carrier-based phase disposition pulse width modulation (PWM) is a common strategy. PWM strategy is implemented by using four triangular carriers and three reference signals. Four carriers with the same frequency, amplitude and phase angle are disposed as the upper and lower four layers, labeled as C_1, C_2, C_3 and C_4, which are symmetrically distributed in the two-side of the horizontal axis, and compared with a sine modulation wave (Fig. 2) [18].

The modulation strategy for NPC five levels inverter (Fig. 3). PWM strategy is applied for arms. In Fig. 4, C_1, C_2, C_3 and C_4 are triangular carriers of three arm (a, b, c), V_a represents modulation wave of arm a. The phase of C_1 and C_2 are opposite with C_3 and C_4. When the value of V_a is higher than C_1, K_1 and C_2, K_2 are switched on. When the value of V_a is lower than C_3, K_3 and C_4, K_4 are switched on. In the other case, K_1, K_2, K_3' and K_4' are turned on, and the output
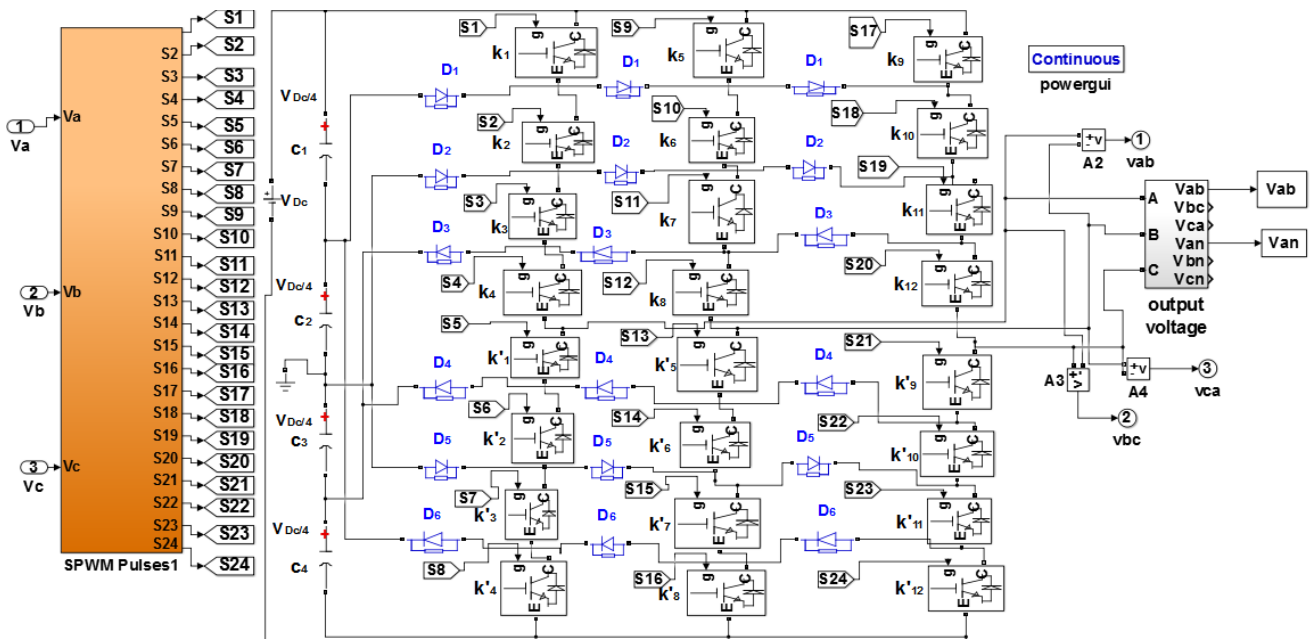
Fig. 1 NPC five-level inverter structure
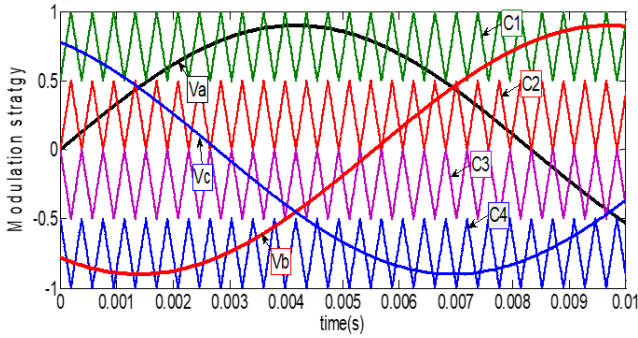
Fig. 2 Modulation strategy of NPC five-levels inverter
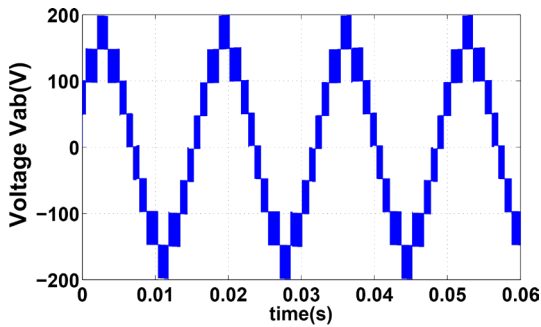
Fig. 3 Output voltage phase of NPC five levels inverter
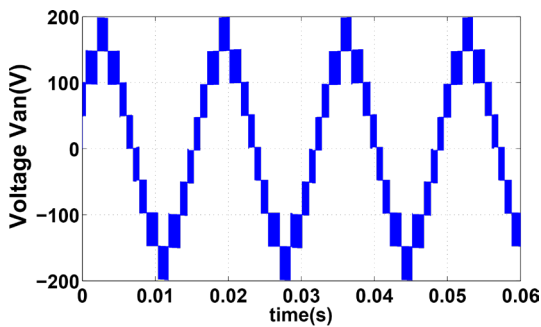
Fig. 4 Output voltage line of NPC five levels inverter
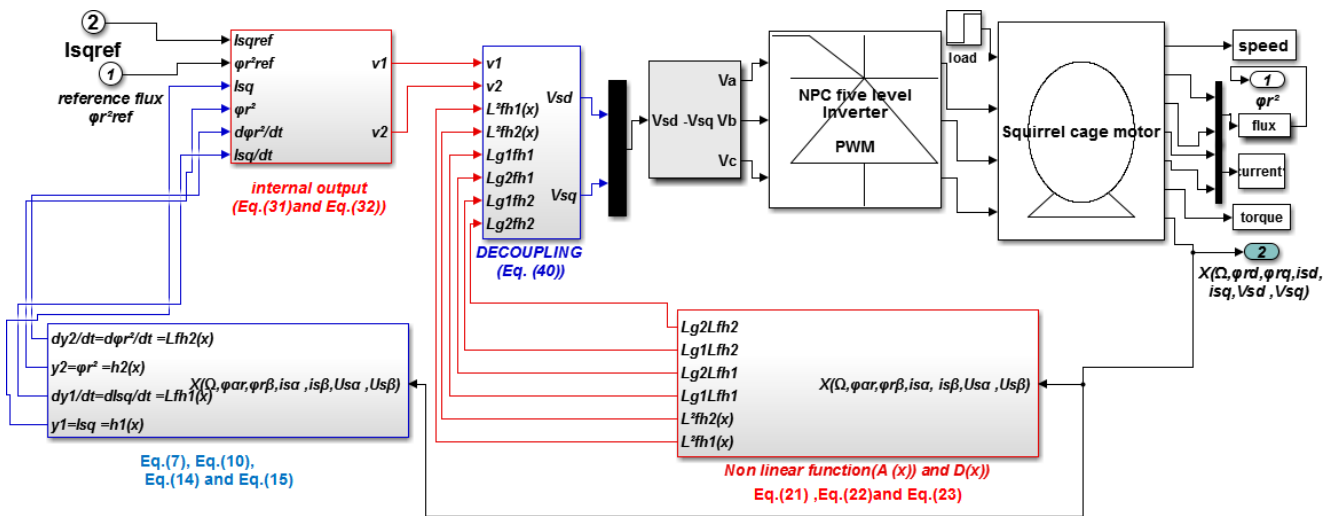
level is 0. Similarly, C_1, C_2, C_3 and C_4 are triangular carriers of arms b and C, V_c represents modulation wave of arm b and V_c represents modulation wave of arm C. Same principle appliqued for arm a is appliqued for two arms b and C [18].

In Figs. 3 and 4 we can clearly observed the five level for one output phase and one output line generated by the NPC inverter. In Fig. 3 the positive voltage levels corresponds to 0, $V_{DC}/4$, $V_{DC}/2$, $3V_{DC}/4$, V_{DC}, all totaling, while the negative output voltage level corresponds to 0, $-V_{DC}/4$, $-V_{DC}/2$, $-3V_{DC}/4$, V_{DC}, all totaling, all totaling to a five levels.

Fig. 5 shows that there are two control inputs for the given system, one control input is used to regulate the input speed Ω and the other is for the flux φ_r^2; we should have two outputs (V_{sd}, V_{sq}) for input-output decoupling.

The input-output linearization control composed for different controls: the first one is the nonlinear functions $A(x)$ and $D(x)$ which are drawn by using Lie derivatives, where $A(x)$ is given by Eqs. (21) and (22) and $D(x)$ is given by Eq. (23). The second controls are the new inputs (V_1, V_2) which are given by Eqs. (31) and (32) and the third command is state space modification of coordinates whish are given by Eqs. (7), (10), (14) and (15).

The final command is decoupling matrix of the input-output linearization control of induction motor which is given by Eq. (40).

7 Speed sliding input-output linearization control

The motor speed Ω should track a specific reference speed Ω_{ref} with presence of load torque [9–11].

The system is controlled in such a way that the error $e(t) = \Omega_{ref} - \Omega$ and its rate of change always move towards

Fig. 5 Input output linearization control of squirrel cage motor

a sliding surface. We take $n = 1$, the speed control manifold equations can be obtained as [11, 12]:

$$S(\Omega) = \Omega_{ref} - \Omega, \tag{53}$$

$$\frac{dS(\Omega)}{dt} = \frac{d\Omega_{ref}}{dt} - \frac{d\Omega}{dt}, \tag{54}$$

$$T_e = \frac{pL_m}{JL_r} \varphi_{rd} I_{sq}, \tag{55}$$

$$\frac{d\Omega}{dt} = \frac{T_e}{J} - \frac{1}{J} T_l - \frac{1}{J} f\Omega. \tag{56}$$

Substituting the expression of T_e defined by Eq. (51) in Eq. (52), we obtain:

$$\frac{d\Omega}{dt} = \frac{pL_m}{JL_r}(\varphi_{rd} I_{sq}) - \frac{1}{J} T_l - \frac{1}{J} f\Omega. \tag{57}$$

Substituting the expression of $d\Omega/dt$ defined by Eq. (53) in Eq. (50), we obtain:

$$\frac{dS(\Omega)}{dt} = \frac{d\Omega_{ref}}{dt} - \frac{pL_m}{JL_r}(\varphi_{rd} I_{sq}) + \frac{1}{J} T_l + \frac{1}{J} f\Omega. \tag{58}$$

Substituting the expression of I_{sq} by the command clearly appears in Eq. (54):

$$\frac{dS(\Omega)}{dt} = \frac{d\Omega_{ref}}{dt} - \frac{pL_m}{JL_r} \varphi_{rd}\left(I_{sq}^{eq} + I_{sq}^{n}\right) + \frac{1}{J} T_l + \frac{1}{J} f\Omega. \tag{59}$$

During the sliding mode and in permanent regime, we have:

$$S(\Omega) = 0, \quad \frac{dS(\Omega)}{dt} = 0, \quad I_{sq}^{n} = 0, \tag{60}$$

where the equivalent control is:

$$I_{sq}^{eq} = \left(\frac{d\Omega_{ref}}{dt} + \frac{1}{J} T_l + \frac{1}{J} f\Omega\right) \frac{JL_r}{n_p L_m} \frac{1}{\varphi_{rd}}. \tag{61}$$

Consider de Lyapunov function:

$$V = \frac{1}{2} S(\Omega)^2. \tag{62}$$

From the Lyapunov theorem, we know that if dv/dt is negative definite, the system trajectory will be driven and attracted toward the sliding surface and remain sliding on it until the origin is reached asymptotically.

$$\frac{dv}{dt} = S(\Omega) \frac{dS(\Omega)}{dt} < 0. \tag{63}$$

During the convergence mode, the condition must be verified. We obtain:

$$\frac{dS(\Omega)}{dt} = -\frac{pL_m}{JL_r} \varphi_{rd}. \tag{64}$$

The correction factor (discontinuous command) gives by Eq. (65):

$$I_{sq}^{n} = K_{q1} sat(S(\Omega)), \tag{65}$$

where:

$$sat(S(\Omega)) = \begin{cases} S(\Omega) & \text{if } |S(\Omega)| < 0 \\ \frac{1}{\delta} S(\Omega) & \text{if } |S(\Omega)| > 0 \end{cases}. \tag{66}$$

Fig. 6 shows a combination between the sliding speed control (SM) and input-output linearization control (IOLC) of squirrel cage motor that gives new controller named
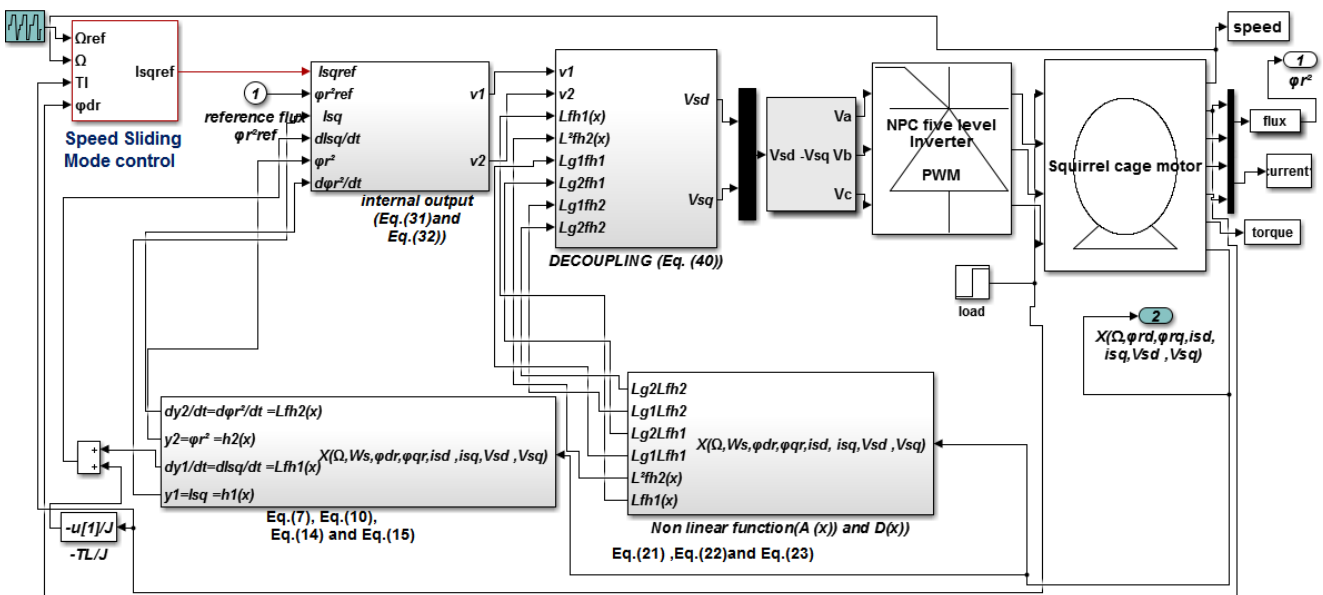
Fig. 6 Block diagram of the sliding input-output linearization control of squirrel cage motor

by sliding input-output linearization control (SIOLC). The output of sliding speed controller delivers a reference current which will be an input for the internal input V_1 of the input-output linearization control of squirrel cage motors.

Fig. 7 shows the subsystem of combination between the sliding speed control and input-output linearization control. The sliding mode control used for controlling speed of squirrel cage motor, the output of this controller is input for input-output linearization control.

8 Result and discussion

In Fig. 8, the machine is applied with a load torque of 10 N m in a time interval [0.26, 0.75] s and [1.91, 2.3] s; the direction of rotation of the machine is reversed from 157 rad/s to −100 rad/s in time 2.79 s. When the motor is started with the reference speed 50 rad/s in the time interval

[0.05, 1] s, it can be seen that in the input-output linearization control the speed returns to its reference after overshooting during the transient regime. When the direction of rotation is reversed, the speed overshoots and then follows its reference in the steady state. The load torque application causes a slight decrease in speed, which is quickly rejected.

The simulation results show that the sliding input-output linearization control (SIOLC) is robust to the variation of the reference speed, since the speed follows the reference speed at start-up as well as the reversal of the direction of rotation, in a very satisfactory way, the application of load torque does not influence the speed response.

In the Fig. 8 (a) and (b) the sliding input-output linearization control (SIOLC) ensures the robustness of this technique to high and low speed variations as well as the application of load torque (T_l = 10 N m) in time interval
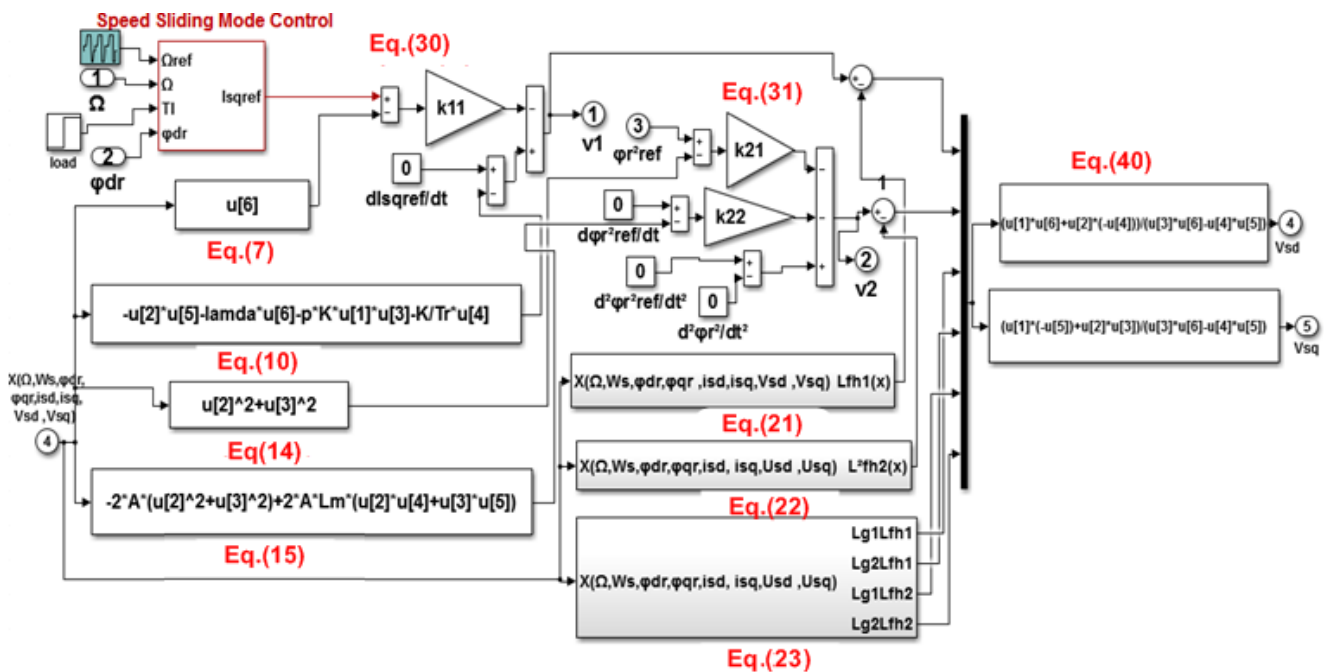
Fig. 7 Subsystem of sliding input-output linearization control
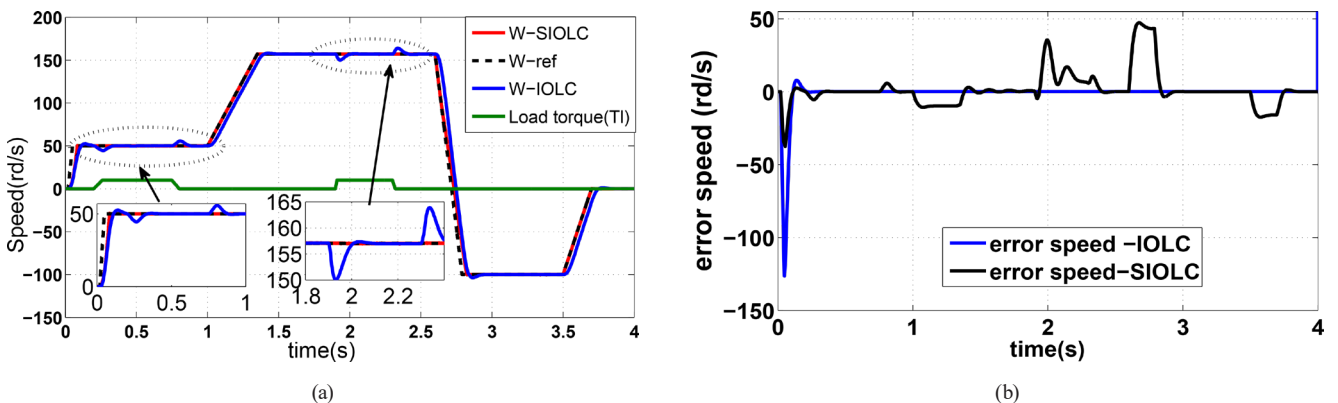
Fig. 8 Speed and error speed response (IOLC, SIOLC); (a) Speed; (b) Error speed

[0.26, 0.75] s and [0.91, 2.3] s. Concerning the input-output linearization control (IOLC) can lead to a degradation of the expected performances mainly regarding the tracking of the reference speed and the application of load torque.

From Figs. 9 and 10, it is clear that SIOLC performs better and is more capable to force flux and torque to track its reference, which means the robustness of SIOLC is stronger in comparison to IOLC that reduces the robustness of the system.

The currents generated by the squirrel cage motor with the IOLC and SIOLC strategies are shown in Fig. 11 (a) and (b). One can clearly see that the SIOLC proposed technique significantly improve the current quality compared to the one obtained with IOLC. We notice that on the zoom of Fig. 11 (a) of rotor current by the strategy of SIOLC control less ripple and oscillation on its response compared to the zoom of Fig. 11 (b) of IOLC control where we observe remarkable ripple on the rotor current response.

Fig. 12 (a) and (b) show the stator currents generated by the squirrel cage motor with the IOLC and SIOLC strategies.

Results obtained from zoom stator current Fig. 12 (a) shows remarkable ripple on the stator current response which is given by the IOLC command, unlike the SIOLC command can see less ripples on the stator current given by
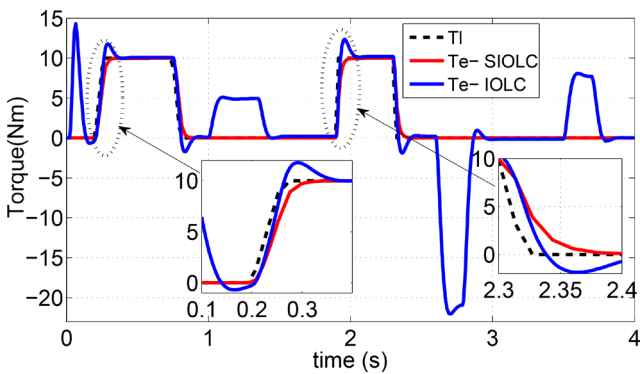
Fig. 9 Electromagnetic torque (IOLC, SIOLC)
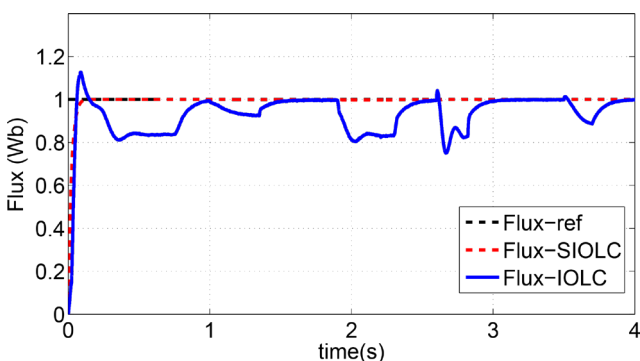
Fig. 10 Electromagnetic flux (IOLC, SIOLC)
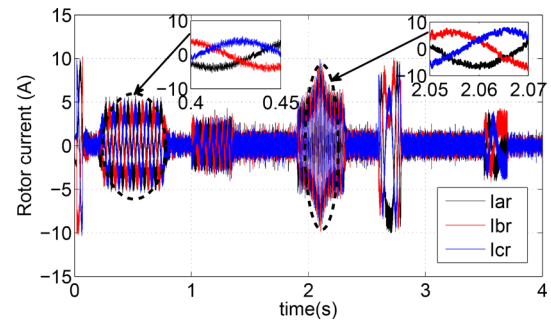
(a)
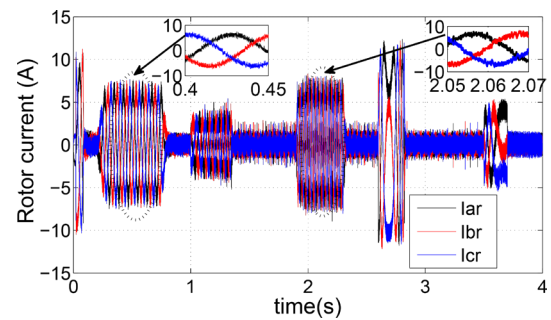
(b)

Fig. 11 Rotor current; (a) IOLC; (b) SIOLC
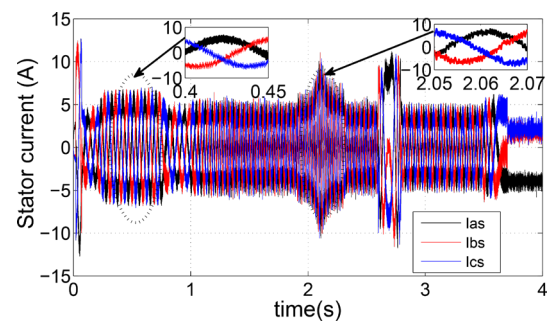
(a)
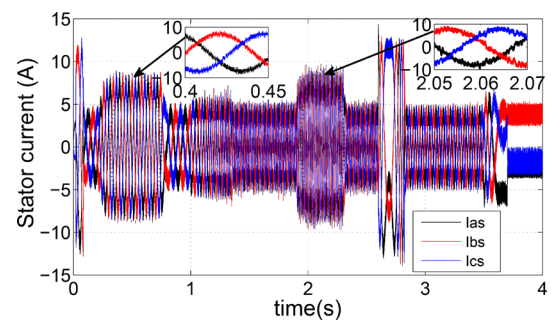
(b)

Fig. 12 Stator current; (a) IOLC; (b) SIOLC

this technique (Fig. 12 (b)), we will conclude that the combination of SMC with the IOLC gives us a new command which is SIOLC which improves the responses of the physical parameters of squirrel cage motor given only by IOLC.

8.1 Test rebstness

The results confirm the performances obtained by SIOLC via the variation of the rotor resistance (R_r) in the time interval [1.2, 2.5] s. Fig. 13 illustrate the dynamic response of the rotor speed of SIOLC and IOLC. SIOLC shows that the speed follows its reference with remarkable accuracy against rotor resistance (R_r) variations at high and low speeds compared by IOLC that we show an undulation and overshoot on speed response.

From Fig. 14, SIOLC shows that the torque response is not influenced by the variation of the rotor resistance compared to IOLC where the torque response contains ripples.

Fig. 15 (SIOLC) shows that the flux response is not influenced by the variation of the rotor resistance compared to IOLC where the flux response decrease during the variation of rotor resistance.

9 Conclusion

Two nonlinear controls are presented in this work to control the asynchronous motor which is directly linked by a five-levels NPC inverter PWM technical for the variation of its speed.

In this paper, we present a study for the combination of two nonlinear controls, one is the sliding mode control and the other is the input-output linearization control to have a control named by the sliding input-output linearization control, the performance of the SIOLC strategy includes the rotor resistance and load torque variations. We validated this method by simulations on a nonlinear model of the squirrel cage motor. The obtained simulation showed that the SIOLC has excellent robustness to parametric uncertainty and disturbances.

The simulation results show that SIOLC is an excellent solution for improving the performance of physical parameters of squirrel cage motor in terms of tracking

Fig. 13 Speed response via rotor resitance variation (R_r)
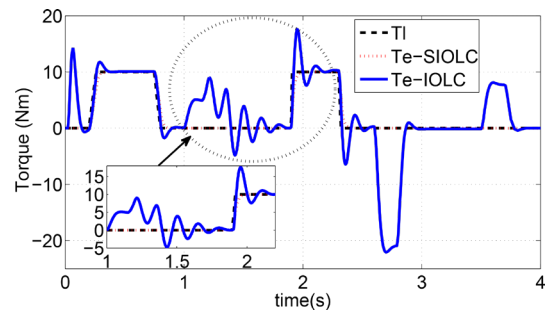
Fig. 14 Torque response via rotor resitance variation (R_r)
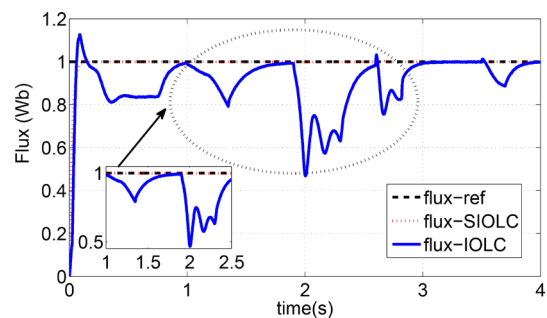
Fig. 15 Flux response via rotor resitance variation (R_r)

performances speed and flux references. Furthermore, the obtained results have approved that with SIOLC the ripples are reduced on the motor stator and rotor current response.

References

[1] Dendouga, A. "Feedback linearization associated to a sliding mode controller for an operating with unity power factor of induction motor fed by matrix converter", SN Applied Sciences, 2(5), 879, 2020.
https://doi.org/10.1007/s42452-020-2674-7

[2] Fetene, Y., Shibeshi, D. "Fractional Order Sliding Mode Speed Control of Feedback Linearized Induction Motor", Power Electronics and Drives, 5(41), pp. 109–122, 2020.
https://doi.org/10.2478/pead-2020-0010

[3] Oukaci, A., Toufouti, R., Dib, D., Atarsia, L. "Comparison Performance between Sliding Mode Control and Nonlinear Control Application to Induction Motor", Electrical Engineering, 99(1), pp. 33–45, 2017.
https://doi.org/10.1007/s00202-016-0376-3

[4] AL-Hashemi, S. A., AL-Dujaili, A., Ajel, A. R. "Speed Control Using an Integral Sliding Mode Controller for a Three-Phase Induction Motor", Journal of Techniques, 3(3), pp. 10–19, 2021.
https://doi.org/10.51173/jt.v3i3.328

[5] Wang, C., Tang, J., Jiang, B., Wu, Z. "Sliding-mode variable structure control for complex automatic systems: a survey", Mathematical Biosciences and Engineering, 19(3), pp. 2616–2640, 2022.
https://doi.org/10.3934/mbe.2022120

[6] Cherifi, D., Miloud, Y. "Robust Speed-sensorless Vector Control of Doubly Fed Induction Motor Drive Using Sliding Mode Rotor Flux Observer", International Journal of Applied Power Engineering (IJAPE), 7(3), pp. 235–250, 2018.
https://doi.org/10.11591/ijape.v7.i3.pp235-250

[7] Venkateswarlu, K., Sandeep, G., Srinivas, N., Reddy, K. D., Ramakrishna, A. "Speed Sensorless Sliding Mode Control of Induction Motor Using Simulink", IOSR Journal of Electrical and Electronics Engineering, 6(2), pp. 50–56, 2013.
https://doi.org/10.979/1676-0625056

[8] Ghozlane, W., Knani, J. "Nonlinear Control via Input-Output Feedback Linearization of a Robot Manipulator", Advances in Science, Technology and Engineering Systems Journal, 3(5), pp. 374–381, 2018.
https://doi.org/10.25046/aj030543

[9] Farrokh Payam, A., Mirzaeian Dehkordi, B., Moallem, M. "Adaptive Input-Output Feedback Linearization Controller for Doubly-Fed Induction Machine Drives", In: 2007 International Aegean Conference on Electrical Machines and Power Electronics, Bodrum, Turkey, 2007, pp. 830–835. ISBN 978-1-4244-0890-0
https://doi.org/10.1109/ACEMP.2007.4510606

[10] Alonge, F., Cirrincione, M., Pucci, M., Sferlazza, A. "Input–output feedback linearization control with on-line MRAS-based inductor resistance estimation of linear induction motors including the dynamic end effects", IEEE Transactions on Industry Applications, 52(1), pp. 254–266, 2015.
https://doi.org/10.1109/TIA.2015.2465939

[11] Marino, R., Peresada, S., Valigi, P. "Adaptive Input-Output Linearizing Control of Induction Motors", IEEE Transactions on Automatic Control, 38(2), pp. 208–211, 1993.
https://doi.org/10.1109/9.250510

[12] Yahiaoui, A., Iffouzar, K., Himour, K., Ghedamsi, K. "Comparison of Different Multilevel Voltages Source Inverter Topologies on Induction Motor Energy Quality", European Journal of Electrical Engineering, 21(4), pp. 367–372, 2019.
https://doi.org/10.18280/ejee.210404

[13] Rasulkhani, A., Taheri, A. "A New Multilevel Inverter Topology with Component Count Reduction", International Journal of Industrial Electronics, Control and Optimization, 2(4), pp. 355–364, 2019.
https://doi.org/10.22111/ieco.2019.28028.1121

[14] Pandian, G., Rama Reddy, S. "Simulation and Analysis of Multi Level Inverter Fed Induction Motor drive", Indian Journal of Science and Technology, 2(2), pp. 67–69, 2009.
https://doi.org/10.17485/ijst/2009/v2i2.6

[15] Elmenofy, G. A., Osheba, D., Elkholy, E., El-Hefnawy, A. "A Proposed Five-level Neutral Point Clamped Inverter", Engineering Research Journal: Scientific Journal of the Faculty of Engineering Menoufia University, 44(2), pp. 135–140, 2021.
https://doi.org/10.21608/erjm.2021.58129.1072

[16] Cherifi, D., Miloud, Y., Mostefai, M. "Performance of Neutral Point Clamped Five Level Inverter Using Space Vector Modulation Control Fed by DPC-VF-SVM Rectifier", WSEAS Transactions on Power Systems, 16, pp. 275–287, 2021.
https://doi.org/10.37394/232016.2021.16.28

[17] Abdel-Rahim, O., Wang, H. "Five-level one-capacitor boost multi-level inverter", IET Power Electronics, 13(11), pp. 2245–2251, 2020.
https://doi.org/10.1049/iet-pel.2020.0033

[18] Benbouhenni, H., Boudjema, Z., Belaidi, A. "Higher Control Scheme Using Neural Second Order Sliding Mode and ANFIS-SVM strategy for a DFIG-Based Wind Turbine", International Journal of Advances in Telecommunications Electrotechnics, Signals and Systems, 8(2), pp. 17–28, 2019.
https://doi.org/10.11601/ijates.v8i2.263

[19] Wang, K., Zheng, Z., Xu, L., Li, Y. "Neutral-Point Voltage Balancing Method for Five-Level NPC Inverters Based on Carrier-Overlapped PWM", IEEE Transactions on Power Electronics, 36(2), pp. 1428–1440, 2021.
https://doi.org/10.1109/TPEL.2020.3006960

[20] Rezki, M., Griche, I. "Simulation and Modeling of a Five-Level (NPC) Inverter Fed by a Photovoltaic Generator and Integrated in a Hybrid Wind-PV Power System", Engineering, Technology & Applied Science Research, 7(4), pp. 1759–1764, 2017.
https://doi.org/10.48084/etasr.1271

Appendix

The main parameters of squirrel cage motor are given in Table A1.

Table A1 Squirrel cage motor parameters

Motor parameters	Value
Number of pairs of poles (p)	2
Rated power (P)	1.5 kW
Stator rated frequency (f)	50 Hz
Stator rated voltage (V_s)	220/380 V
Stator inductance (L_s)	0.274 H
Rotor inductance (L_r)	0.274 H
Mutual inductance (L_m)	0.258 H
Stator inductance (R_s)	3.805 Ω
Rotor inductance (R_r)	4.81 Ω